

Spiking Neural Networks for Handwritten Digit Recognition – Supervised Learning and Network Optimization

Shruti R. Kulkarni^a, Bipin Rajendran^{a,*}

^a*Department of Electrical and Computer Engineering, New Jersey Institute of Technology, NJ, 07102 USA*

Abstract

We demonstrate supervised learning in Spiking Neural Networks (SNNs) for the problem of handwritten digit recognition using the spike triggered Normalized Approximate Descent (NormAD) algorithm. Our network that employs neurons operating at sparse biological spike rates below 300 Hz achieves a classification accuracy of 98.17% on the MNIST test database with four times fewer parameters compared to the state-of-the-art. We present several insights from extensive numerical experiments regarding optimization of learning parameters and network configuration to improve its accuracy. We also describe a number of strategies to optimize the SNN for implementation in memory and energy constrained hardware, including approximations in computing the neuronal dynamics and reduced precision in storing the synaptic weights. Experiments reveal that even with 3-bit synaptic weights, the classification accuracy of the designed SNN does not degrade beyond 1% as compared to the floating-point baseline. Further, the proposed SNN, which is trained based on the precise spike timing information outperforms an equivalent non-spiking artificial neural network (ANN) trained using back propagation, especially at low bit precision. Thus, our study shows the potential for realizing efficient neuromorphic systems that use spike based information encoding and learning for real-world applications.

*Corresponding author
Email address: bipin@njit.edu (Bipin Rajendran)

Keywords: Neural networks, spiking neurons, supervised learning, pattern recognition, approximate computing, neuromorphic computing

¹ **1. Introduction**

² The superior computational efficiency of biological systems has inspired the
³ quest to reverse engineer the brain in order to develop intelligent computing
⁴ platforms that can learn to execute a wide variety of data analytics and in-
⁵ ference tasks [1]. Artificial neural networks (ANNs), inspired by the network
⁶ architecture of the brain, have emerged as the state-of-the-art for various ma-
⁷ chine learning applications. In particular, inspired by the Nobel prize winning
⁸ work of Hubel and Weisel on elucidating the mechanisms of information rep-
⁹ resentation in the visual cortex [2], multi-layer convolutional neural networks
¹⁰ have shown impressive performance for a wide variety of applications such as
¹¹ image recognition, natural language processing, speech recognition and video
¹² analytics [3, 4, 5, 6, 7, 8, 9, 10, 11].

¹³ Nevertheless, the neurons in ANNs implement a memoryless nonlinear trans-
¹⁴ formation of the input synaptic signals to create real-valued output signals. This
¹⁵ is vastly different from the behavior of neurons in the brain, which encode infor-
¹⁶ mation in the timing of binary signals, called action potentials or spikes based
¹⁷ on the timing of incoming spike signals from upstream nodes. The third gener-
¹⁸ ation of artificial neural networks, also called spiking neural networks (SNNs),
¹⁹ have been introduced to mimic this key aspect of information processing in the
²⁰ brain [12]. There is growing evidence that SNNs have significant computational
²¹ advantages as a result of their higher information representational capacity due
²² to the incorporation of the temporal dimension [13, 14, 15, 16]. Furthermore,
²³ SNNs issue spikes sparsely - the observed spike rate in biological networks is
²⁴ in the range of 0.1 to 300 Hz - and they operate in an event-driven manner
²⁵ [17, 18, 19, 20]. Therefore, highly energy efficient neuromorphic systems can be
²⁶ realized in hardware based on SNNs, as is evidenced by recent demonstrations
²⁷ [21, 22, 23, 24, 25].

28 Earlier efforts to build learning algorithms for SNNs were inspired by recent
29 discoveries from neuroscience that shed light on the synaptic (neuronal inter-
30 connections) mechanisms of adaptation based on the difference in the times of
31 issue of pre- and post-synaptic spikes. The most prominent among them is the
32 Remote Supervised Method (ReSuMe) [26], that adjusts the synaptic weights
33 based on the precise timing differences of the input and output neurons, in-
34 spired by the spike timing dependent plasticity (STDP) rule. Other spike based
35 learning algorithms that have been proposed include the SpikeProp algorithm
36 (though it was restricted to single spike learning) [27], SPAN and PSD, which
37 converted spikes to smoothed analog signals and defined a continuous time
38 cost function for training [28, 29]. Another important spike based supervised
39 learning rule was the Chronotron rule which used piece-wise gradient descent
40 and was demonstrated to be efficient in identifying different classes of random
41 spike trains [30]. Recently, the reward modulated STDP or R-STDP learning
42 has shown superior performance on several benchmark problems compared to
43 STDP SNNs and even traditional CNNs, even though training was limited to
44 a single layer in the network [31]. A variant of ReSuMe algorithm, called the
45 Delay Learning (DL)-ReSuMe, in addition to the synaptic weights, made use of
46 the transmission delays of synapses interconnecting the neurons as parameters
47 to train the network [32]. This algorithm has been shown to be superior in terms
48 of accuracy and speed of convergence compared to the basic ReSuMe algorithm.
49 The accurate synaptic efficiency adjustment method is another spike-error trig-
50 gered supervised learning rule based on STDP, which optimizes a cost function
51 defined in terms of membrane potential differences [33]. This method has been
52 used to demonstrate excellent performance in several UCI datasets with few
53 training parameters. The Synaptic Kernel Inverse Method (SKIM) [34], eval-
54 uates the weights analytically rather than learning them iteratively and has been
55 applied to the problem of speech based digit recognition in a small network
56 with 50 neurons. Based on the SKIM method, the convex optimized synaptic
57 efficiencies (CONE) algorithm was developed [35] and was used for the prob-
58 lem of gait detection. The generalization capability of this algorithm and the

59 noise tolerance of a variation of the algorithm called CONE-R has also been
60 demonstrated.

61 Our work focuses on applying a precise spike based supervised learning algo-
62 rithm to the MNIST (Modified National Institute of Standards and Technology
63 database) handwritten digit classification problem and optimizing the network
64 in terms of the number of learning parameters for implementation in energy and
65 memory constrained hardware.

66 In addition to the above mentioned learning methods, unsupervised learning
67 algorithms for SNNs have also been explored, based on the biological spike
68 timing dependent plasticity (STDP) rule [36, 37, 38, 39, 40, 41, 42]. While
69 these networks use multi-layered convolution architectures with more than one
70 million parameters and have achieved over 98% accuracy on the MNIST dataset
71 [38, 39], we demonstrate similar accuracy with 13 \times fewer parameters.

72 There are also several efforts directed towards developing architectures with
73 adaptive and evolving network structures [43, 44, 45, 46, 47]. SpikeTemp and
74 SpikeComp are algorithms where neurons are progressively added in the classi-
75 fier layer as the training algorithm approaches the optimal point [45, 46]. The
76 recently developed evolving architecture called NeuCube, directly inspired by
77 the brain [43], incorporates weight adjustments based on supervised and un-
78 supervised rules and additionally, adds new network neurons as per training
79 requirements.

80 Besides the above-mentioned approaches for designing learning algorithms
81 for SNNs that operate directly in the spike domain, several authors have pro-
82 posed to convert ANNs trained with the well-established backpropagation algo-
83 rithm to SNNs so that the latter can be used as inference engines [48, 49, 50,
84 51, 52, 53]. ANN-to-SNN conversion imposes that the firing rate of a spiking
85 neuron in the SNN be proportional to the activation output of a non-spiking
86 neuron in the ANN. Various techniques such as approximating the response of a
87 spiking neuron with a smooth differentiable ReLU-like function, weight normal-
88 ization, noise addition, lateral inhibition or spiking rate based pooling masks,
89 which is similar to max pooling operation, have been employed to this end.

90 Using these approaches, state-of-the-art inference accuracies have been demon-
91 strated in spike domain equivalent of deep learning networks such as VGG-16
92 and Inception-V13 for ImageNet classification problem, and close to $2\times$ reduc-
93 tion in the number of operations needed compared to CNNs for smaller problems
94 such as MNIST and CIFAR-10 [53]. Recently, a more biologically plausible al-
95 gorithm called the Feedback Alignment (FA) has been proposed, which unlike
96 the standard backpropagation uses two different sets of weights in the feed-
97 forward and feedback paths [54]. This method has also been demonstrated
98 in SNNs, using approximate differentiable functions of leaky integrate and fire
99 (LIF) spiking neurons to train them in an online manner. However, the FA rule
100 has lower performance compared to the standard backpropagation rule [52].

101 Towards the goal of demonstrating a learning SNN capable of high accuracy
102 and efficiency, we use the recently proposed Normalized Approximate Descent
103 (NormAD) algorithm to train the output layer weights of a three-layered net-
104 work with fixed convolutional kernel weights in the hidden layer. This spike-
105 triggered weight update rule frames the learning task as a supervised optimiza-
106 tion problem aimed at tuning the membrane potential to create spikes at desired
107 time instants. Compared to other deterministic learning algorithms in the spike
108 domain such as ReSuMe, at least $10\times$ faster convergence characteristics have
109 been demonstrated using this algorithm for generating arbitrarily desired spike
110 streams [55].

111 Prior SNN based demonstration of handwritten digit recognition using spik-
112 ing versions of backpropagation of errors has achieved 98.7% based on a fully
113 connected 4-layer network and 99.31% with convolutional spiking networks, but
114 also with more than $4\times$ higher number of trainable synapses compared to our
115 network [56]. The training algorithm employed in that work has a cost function
116 that is continuous in time defined in terms of the low pass filtered spike trains
117 (both input and output). Compared to the state-of-the-art networks which have
118 shown over 99% accuracy, our SNN trained with NormAD shows an accuracy of
119 98.17% on the test set of the MNIST database, with $4\times$ fewer synaptic learning
120 parameters [3, 4, 11, 56]. Furthermore, if the network architecture and number

121 of synaptic parameters are kept the same, we show that the accuracy and perfor-
122 mance of the NormAD trained SNN is slightly better than that of an equivalent
123 ANN trained using backpropagation.

124 This paper is organized as follows. We introduce the basic units of SNNs
125 in Section 2. Section 3 describes the architecture of our network, the spike en-
126 coding at the input and output of the network, and the training algorithm used
127 for weight updates. Section 4 describes several hyper-parameter tuning exper-
128 iments and the results achieved on the MNIST database. Section 5 discusses
129 the optimization of the network for implementation in energy and memory con-
130 strained hardware platforms by approximating the neuronal dynamics and using
131 low-precision bits for storing the synaptic weights. Finally, section 6 summarizes
132 the key conclusions of our work.

133 2. Spiking Neural Networks

134 SNNs are the third generation of neural networks employing neuron models
135 that are inspired by the biological mechanisms of neuronal signaling. While the
136 mechanism of spike process in biological neurons depends on complex interac-
137 tions of ion-channels on the cell membrane, a computationally simpler leaky
138 integrate and fire (LIF) model is typically used for simulation of spiking neural
139 networks [57]. This model represents the potential of a neuron as the voltage
140 across a capacitor connected in parallel with a leaky conductance path, and is
141 charged by incoming input currents. Accordingly, the membrane potential $V(t)$
142 evolves according to the differential equation:

$$143 C \frac{dV(t)}{dt} = -g_L(V(t) - E_L) + I_{syn}(t). \quad (1)$$

144 When $V(t) \geq V_T$, a spike is issued and transmitted to the downstream synapses;
145 the membrane potential is reset to its resting value E_L after the spike. We use
146 $E_L = -70$ mV and $V_T = 20$ mV in our simulations. $C = 300$ pF and $g_L =$
147 30 nS model the membrane's capacitance and leak conductance, respectively.
148 Biological neurons enter a refractory period immediately after a spike is issued

149 during which another spike cannot be issued. We implement this by holding the
150 membrane potential at $V(t) = E_L$ for a short period $t_{ref} = 3$ ms after the issue
151 of a spike. We also limit the membrane potential to the range $[E_L, V_T]$ through
152 clipping.

153 The spikes arriving at a synapse having a strength (weight) w , will gener-
154 ate a post-synaptic current ($I_{syn}(t)$) in its downstream neuron, given by the
155 expressions:

$$\small 156 \quad c(t) = \sum_i \delta(t - t^i) * \left(e^{-t/\tau_1} - e^{-t/\tau_2} \right) \quad (2)$$

$$\small 157 \quad I_{syn}(t) = w \times c(t). \quad (3)$$

158 where t^i denotes the time of issue of the i^{th} incoming spike and $*$ is the convo-
159 lution operator. The variables $\tau_1 = 5$ ms and $\tau_2 = 1.25$ ms model the shape of
160 the synaptic current kernel $c(t)$ and denote its falling and rising time constants,
161 respectively. Note that the time of issue of spikes of a LIF neuron depends on
162 the incoming spike times and synaptic strength in a strong nonlinear fashion,
163 due to the weighted summation, integration and reset.

164 3. Network Architecture

165 As illustrated in Fig. 1, we designed a simple 3-layer SNN for classification of
166 handwritten digits from the MNIST database. Since MNIST images are 28×28
167 pixels, our network's input layer has 784 neurons and the output layer has 10
168 neurons, each corresponding to a particular digit. The input layer neurons
169 connect to 8112 hidden layer neurons through twelve *a priori* fixed 3×3 sized
170 convolutional kernels. The synapses connecting this hidden layer to the output
171 layer are trained using the NormAD algorithm.

172 3.1. Input encoding

173 Biological sensory neurons employ complex transformations such as rate
174 coding, time-of-spike coding, population coding and phase coding to encode
175 real-world information in the spike domain [58]. Time-encoding machines that

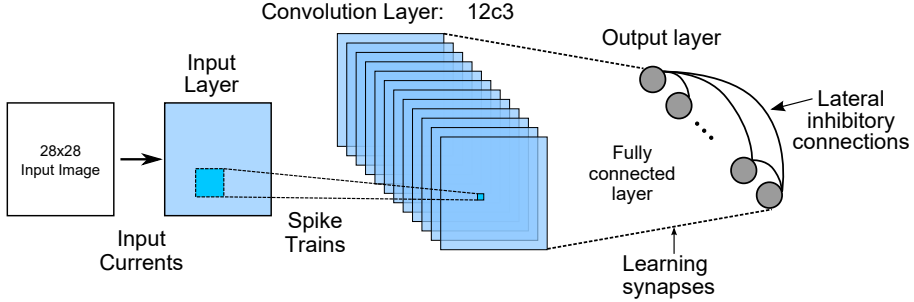


Figure 1: The proposed spiking neural network architecture for handwritten digit classification. The spike trains from the input layer with 28×28 neurons are spatially convolved with twelve filters (or convolution kernels) of size 3×3 , resulting in the twelve feature maps of size 26×26 . The synapses connecting the 8112 convolution layer neurons and the 10 output layer neurons are tuned during training. There is a fixed winner-take-all (WTA) lateral inhibition between the neurons in the output layer.

176 convert band-limited input signals to the spike domain such that their perfect
 177 reconstruction is possible have been proposed in [59]. There are also some re-
 178 cent works that use Gaussian receptive fields or Poisson encoding to directly
 179 translate real-valued inputs to spike times [60, 40]. As we are dealing with
 180 static images, we translate each gray-scale pixel value, in the range $[0, 255]$, to
 181 currents that can be applied as inputs to the spiking neurons. Accordingly, each
 182 pixel value k is converted into a constant input current for the LIF neuron as:

$$i(k) = I_0 + (k \times I_p). \quad (4)$$

184 where $I_p = 101.2 \text{ pA}$ is a scaling factor and $I_0 = 2700 \text{ pA}$ is the maximum
 185 constant amplitude current that does not generate a spike in the LIF neuron in
 186 equation 1. As a result, a LIF neuron in the input layer issues spikes that are
 187 uniformly spaced in time, with a frequency that is sub-linearly proportional to
 188 the magnitude of its input current [61].

189 3.2. Convolutional feature extraction

190 The convolution layer of our network uses *a priori* determined fixed weights
 191 for the different feature maps and serves to detect the key features of the image.

192 The filter kernels are continuous curves as shown in Fig. 2(left), and incorporate
 193 both excitatory and inhibitory connections. Our kernels are only 3×3 pixels
 194 and were inspired by biological studies that suggest that the first few layers of
 195 the visual cortex consist of small-sized visual receptive fields [2].

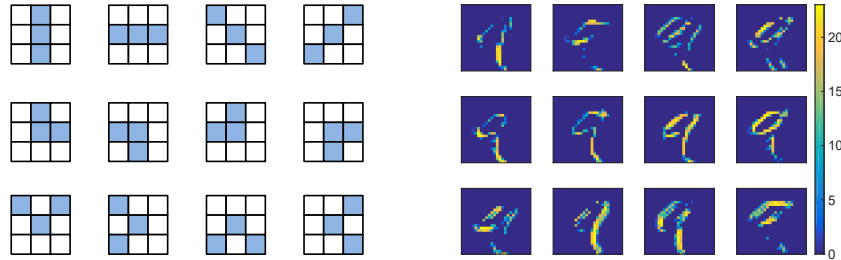


Figure 2: (left) Convolution filters used in our SNN are of size 3×3 pixels. The blue pixels are the excitatory weights, while white pixels are inhibitory values. The magnitude of the excitatory weight is 1.6 times that of the inhibitory weight. (right) The twelve spike count feature maps corresponding to these filters obtained when an exemplary image of digit '9' was presented to the network. The color intensities in the 2D map depict the number of spikes generated by the neurons of the hidden layer when the input was presented for $T = 100$ ms.

196 The filter kernels are spatially convolved with 28×28 spike trains arriving
 197 from the input layer neurons, over a simulation period T , with a stride of 1,
 198 resulting in feature maps of size 26×26 . The weight kernels have an overall
 199 net higher inhibition than excitation, as it helped to better suppress the spikes
 200 from unwanted edges of the input digit image in the corresponding feature map.
 201 Fixed weights based on Gabor filters have been used before as the first layer
 202 in a deep convolution neural network, and have shown an improvement in the
 203 accuracy for the MNIST dataset compared to the original LeNet-5 network
 204 [3, 62]. We use relatively simpler edge detection filters in the hidden layer of
 205 our network.

206 The spikes from the input layer neurons pass through these synaptic weight
 207 kernels to generate currents to the hidden layer neurons. The magnitude of the
 208 current entering the hidden layer neurons is scaled such that on an average their
 209 output spike rate is limited to 10 Hz. Fig. 2(right) shows the 2D feature maps
 210 depicting the number of spikes generated by the neurons in the hidden layer

211 when an exemplary image of digit 9 from the MNIST data-set is presented to
 212 the network for $T = 100$ ms. The different kernels are able to effectively encode
 213 the edges and features of the input image in spike domain.

214 *3.3. Learning layer*

215 The synaptic weights connecting the hidden layer to the output classifier
 216 layer are trained using the NormAD algorithm [55]. The weights are initialized
 217 to zero at the beginning of training. Weights of all the 8112×10 synapses in
 218 this fully-connected layer of the network are updated at the end of presentation
 219 of each image, which lasts for the interval T , as:

$$220 \quad \mathbf{w}(n+1) = \mathbf{w}(n) + \Delta\mathbf{w}. \quad (5)$$

221 The weight update, $\Delta\mathbf{w}$ is calculated only when there is a discrepancy be-
 222 tween the spike times in the desired ($S^d(t)$) and observed ($S^o(t)$) spike trains,
 223 $e(t) = S^d(t) - S^o(t)$. As described in [55], this is achieved by defining a cost func-
 224 tion in terms of the error between the desired ($V_{des}(t)$) and observed ($V(\mathbf{w}, t)$)
 225 neuron membrane potentials as:

$$226 \quad J(\mathbf{w}) = \frac{1}{2} \int_0^T |e(t)| (V_{des}(t) - V(\mathbf{w}, t))^2 dt \quad (6)$$

227 Using gradient descent on the instantaneous cost $J(\mathbf{w}, t)$ obtained by restricting
 228 the limits of integral in equation 6 to an infinitesimally small interval around
 229 time t , the instantaneous weight update term can be written as:

$$230 \quad \Delta\mathbf{w}(t) = \eta(t) \nabla_{\mathbf{w}} J(\mathbf{w}, t) \quad (7)$$

231 with

$$232 \quad \nabla_{\mathbf{w}} J(\mathbf{w}, t) = |e(t)| (V_{des}(t) - V(\mathbf{w}, t)) \nabla_{\mathbf{w}} V(\mathbf{w}, t) \quad (8)$$

233 $\eta(t)$ is a time dependent proportionality constant in equation 7. By *normalizing*
 234 and *approximating* the dependence of membrane potential on the weights, it is
 235 possible to obtain a closed form relationship for the weight update as:

$$236 \quad \Delta\mathbf{w} = r \int_0^T e(t) \frac{\hat{\mathbf{d}}(t)}{\|\hat{\mathbf{d}}(t)\|} dt \quad (9)$$

237 where,

238
$$\hat{\mathbf{d}}(t) = \mathbf{c}(t) * \hat{h}(t), \text{ with } \hat{h}(t) = \exp(-t/\tau_L)u(t). \quad (10)$$

239 Here, $c(t)$ is the synaptic kernel as described in equation 2 and $u(t)$ is the
240 Heaviside step function. The constant $\tau_L = 1$ ms represents the approximation
241 for the neuronal time constant, during training phase. Normalization helps in
242 eliminating the dependency on $V_{des}(t)$, which is an unknown term. The weight
243 update depends only on the output spike error $e(t)$ and the incoming spike
244 trains, captured in $\hat{d}(t)$. The constant r , having the dimensions of synaptic
245 conductance, is a function of the number of input neurons, and is set to 200 pS
246 for our network with 8112 incoming synapses per output neuron.

247 In our network, the desired signal $S^d(t)$ for the label neuron is a uniform
248 spike train with a frequency of 285 Hz, corresponding to a spike every 3.5 ms,
249 which is slightly higher than the LIF refractory period of 3 ms. There are no
250 spikes in the $S^d(t)$ for all the other neurons.

251 *3.4. Lateral inhibition at the output layer*

252 In addition to the feed-forward inputs from the convolution layer neurons,
253 each output layer neuron also receives lateral inhibitory inputs from the remain-
254 ing 9 output neurons, implement winner-take-all (WTA) dynamics, similar to
255 [56]. When a neuron spikes, its outgoing WTA synapses inject a negative current
256 to other neurons, thereby suppressing their spikes, as illustrated in Fig. 3.

257 *3.5. Training methodology*

258 During training, each image is presented to the network for a duration T and
259 all the output layer weights are updated after every image, similar to a stochastic
260 gradient descent (SGD) rule. We divide the MNIST training set into two parts:
261 50,000 for training and remaining 10,000 for validation. In each training epoch,
262 all the 50,000 images are presented once to the network. All the neurons'
263 membrane potentials are initialized to their resting value of $E_L = -70$ mV and
264 the synaptic current variables are cleared at the beginning of each simulation.

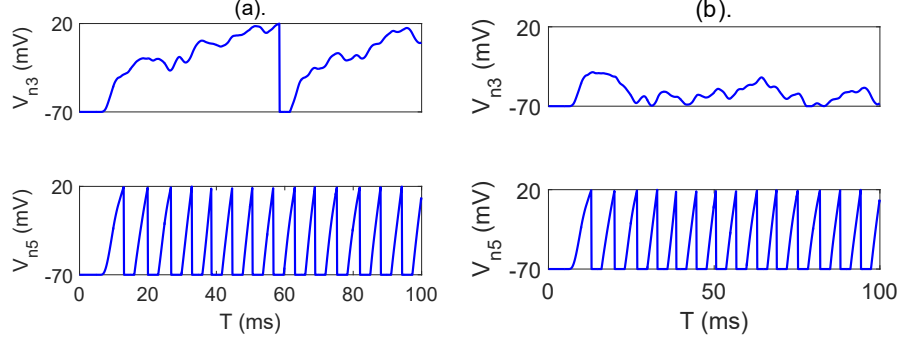


Figure 3: Membrane potential of two output layer neurons ‘3’ and ‘5’, when an input image of digit ‘5’ was presented to the network. (left) Membrane potential without lateral inhibition and (right) with lateral inhibition. It can be seen that lateral inhibition has suppressed the incorrect neuron ‘3’ from issuing a spike.

265 The dynamics of the SNN is evaluated by numerical integration with a time-
 266 step of $\Delta t = 0.1$ ms which is 10 times smaller than the learning time constant,
 267 $\tau_L = 1$ ms used in the NormAD algorithm (see section 3.3). The validation set
 268 is used to tune the hyper-parameters of the network such as the variation in
 269 the learning rate, optimal number of convolution kernels and the presentation
 270 duration as discussed in the following subsections. The network accuracy was
 271 determined on the MNIST test set consisting of 10,000 images. The details of
 272 the GPU implementation of the algorithm are available in the supplementary
 273 material.

274 **4. Results**

275 We now discuss the results of various experiments that we conducted in our
 276 study to optimize the performance of our network. We start with the baseline
 277 experiments that were conducted to analyze network performance, and then
 278 discuss the sensitivity of the network to signal encoding parameters such as
 279 image presentation duration, learning rate schedules and the network size.

280 4.1. Accuracy metrics in spike domain

281 We primarily used two metrics to measure the accuracy of our network –
282 the first based on the spike count and the second based on the correlation C , of
283 the observed spike trains with respect to a reference spike train. In the count
284 metric, the network’s output is decided based on the neuron having the highest
285 spike count. The spike correlation measure [63] between the output spike train
286 $S_i^o(t)$ for each neuron i in the output layer and a reference spike train $S^r(t)$ is
287 defined as:

$$288 \quad C_i = \frac{\langle L[S_i^o(t)], L[S^r(t)] \rangle}{\|L[S_i^o(t)]\| \|L[S^r(t)]\|} \quad (11)$$

289 where

$$290 \quad L[S(t)] = S(t) * \exp(-t/\tau)u(t). \quad (12)$$

291 Here $\langle \mathbf{x}, \mathbf{y} \rangle$ represents the dot product of vectors \mathbf{x} and \mathbf{y} . The training signal
292 with a frequency $f_{out} = 285$ Hz is also used as the reference signal during in-
293 ference. The neuron with the highest value of C is declared the winner of the
294 classification.

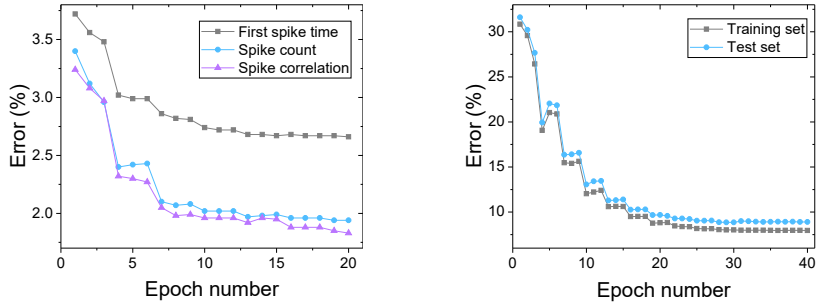


Figure 4: (left) The 3-layer SNN error on the MNIST test data-set based on the count, correlation and first-spike-time metrics. It can be seen that the network classification error in terms of first neuron to spike (in gray) during the presentation interval T , is worse by almost 1% compared to either count (blue) or the correlation metric (magenta). (right) For a 2-layer SNN without the hidden layer, the error saturates to about 8%, even at 40 epochs of training, illustrating the importance of the hidden layer.

295 The SNN is trained on the MNIST training set for 20 epochs. It can be seen
296 from Fig. 4 (left) that precise timing of spikes measured using the correlation

297 metric gives a slightly higher accuracy for classification, though the spike count
298 metric is a simpler metric to evaluate. The classification accuracy of the network
299 is reported using the correlation metric for the succeeding sections in this paper,
300 with explicit mention of the count metric whenever it is used. We also considered
301 the classification accuracy based on the output neuron that spiked first during
302 the input presentation. However, the accuracy based on this metric at the
303 end of 20 epochs was only about 97.34%. While there is a significant drop in
304 accuracy compared to the correlation and spike count metrics, the prediction
305 can be made within 20 ms of image presentation in 99% of input samples using
306 the first-to-spike metric. This trade-off between latency and accuracy may be
307 especially attractive for low-power approximate computing applications.

308 We also note the crucial role the convolutional hidden layer plays in improv-
309 ing the network accuracy – in a 2-layer network with the 784 input neurons
310 connected directly to the 10 output layers, the network’s error saturates around
311 8% (Fig. 4(right)).

312 *4.2. Learning rate schedule optimization*

313 As discussed in [55], the optimal learning rate for the NormAD algorithm
314 depends on the number of input neurons, N_{inp} and scales according to a $N_{inp}^{-1/2}$
315 rule. We studied several protocols (learning rate schedules) to decrease the
316 learning rate during training (Table 1), which resulted in lowering the network
317 error by nearly 0.5% (Fig. 5).

318 Epoch dependent learning rate schedules have shown accuracy improvement
319 in previous works for ANN training [3, 64, 56]; in our study, we experimented
320 with these and several other schedules, shown in the Table 1. We use sched-
321 ule 5 which gave the best validation error after convergence, for the rest of
322 experiments in the paper.

323 *4.3. Network parameter optimization*

324 We also optimized the design parameters of the network such as the number
325 of the convolution kernels used in the hidden layer and the time period T used

Table 1: Learning rate schedules

Scheme	Learning rate (pS)
Schedule 1	$r_0 = 200$, constant over all epochs, n
Schedule 2	$(1/n)$ decrease: $r(n) = \frac{r_0}{(1+k \times n)}$
Schedule 3	Exponential decrease: $r(n) = r_0 \exp(-k \times n)$
Schedule 4	Step decrease by half every 5 epochs
Schedule 5	Step decrease by half every 3 epochs

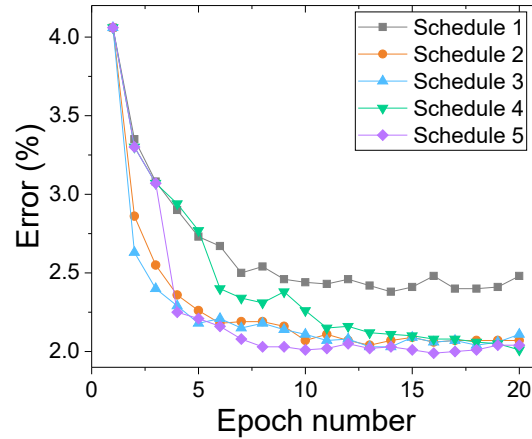


Figure 5: Network error on the validation set for five different rate schedules listed in Table 1.

326 for presenting each input image to the network. Increasing T results in longer
 327 integration time to learn the features of each image, as more spikes (or error
 328 points) are produced, resulting in a larger magnitude for the weight update.
 329 However, from the perspective of improving the throughput for network perfor-
 330 mance and preventing over-fitting, smaller values of T are more desirable. Fig. 6
 331 shows the network performance as a function of the number of convolution ker-
 332 nels and the presentation duration T for the images. The network accuracy is
 333 optimized with 12 kernels and a presentation duration of $T = 100$ ms. We used
 334 a constant inhibitory WTA synaptic strength of 1 nS for all connections in the
 335 output layer.

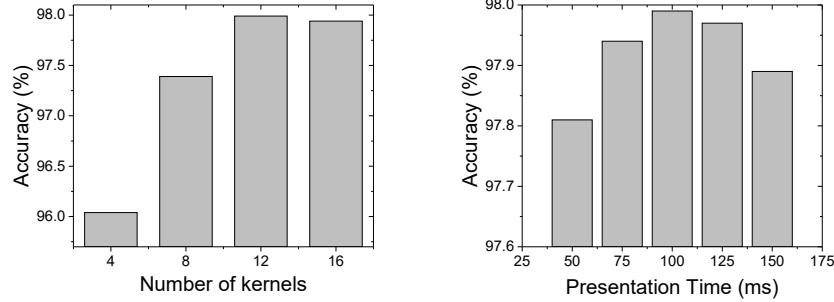


Figure 6: (left) Classification accuracy on the MNIST test set as a function of the number of convolutional kernels; (right) the presentation duration, T . The network accuracy is optimized with 12 kernels and a presentation duration of $T = 100$ ms.

³³⁶ 4.4. *MNIST accuracy results*

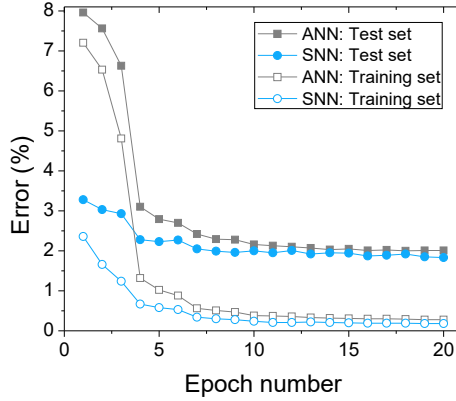


Figure 7: Comparison of the MNIST error for the 3-layer SNN and an equivalent ANN with the same network structure during 20 epochs of training. The SNN performance (0.18% error for training set and 1.83% error for test set at convergence) is slightly better than that of the ANN (0.28% error for training set and 2.0% for test set at convergence).

³³⁷ Having optimized the network hyper-parameters, we trained our SNN with
³³⁸ the complete MNIST dataset (60,000 images) for 20 epochs. The SNN achieved
³³⁹ an accuracy of 99.82% on the MNIST training set and 98.17% on the test set.

³⁴⁰ We also trained an equivalent ANN with the same architecture, i.e., the

341 same number of neurons and connectivity patterns (but without the lateral
 342 WTA connection) as the SNN in Fig. 1. We used the rectified linear unit
 343 (ReLU) as the activation function of the neurons in this network. The weights
 344 of the fully-connected layer were adjusted by the standard gradient descent
 345 rule by back-propagating the network error. After fine-tuning the learning rate
 346 schedule, this ANN achieved an accuracy of 98.0% on the MNIST test set, which
 347 is close to the best case accuracy of around 98.50% reported on an equivalently
 348 sized three-layered ANN [65]. The performance for training and test sets for
 349 the SNN and ANN networks for 20 epochs of training is shown in Fig. 7. This
 350 comparison shows that SNNs trained using the NormAD algorithm can obtain
 351 performance similar to equivalent ANNs in benchmark classification problems.

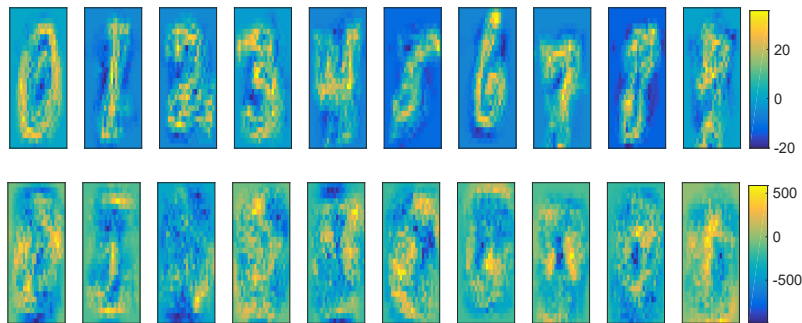


Figure 8: The average of the trained weights (in pS) from the 12 kernels in the hidden layer to the 10 neurons in the output layer is the effective internal representation of the digits learned by the network. (Top) The average weights in the output layer of the SNN after 100 images presented once for training (when the test set accuracy was only 65.8%) and; (Bottom) average weights after training (i.e., with 98.17% accuracy).

352 Fig. 8 shows the average of the trained weights of the synapses from the 12
 353 feature maps to each of the 10 output neurons of SNN. When the network is
 354 trained on the first 100 images, the weight maps closely resemble the images
 355 of the training set digits, though the test set accuracy using these weights was
 356 only about 65.8%. When the network is trained with all the 60,000 images in
 357 the training set, the test set accuracy rises to 98.17%, thanks to a more complex
 358 representation of the images that are captured by the synaptic weights in the

359 network.

Table 2: MNIST classification accuracy comparison - our network architecture achieves over 98% accuracy with atleast four times fewer parameters than the state-of-the-art networks.

Network and learning algorithm (BP stands for back-propagation)	Number of learning synapses	Test set Accuracy
ANN (LeNet-5) [3]	331,984	99.05%
GCNN (LeNet-5 + Gabor filters) [62]	331,984	99.32%
MCDNN (Multi-column Deep NN) [4]	1,574,600	99.77%
DNN with DropConnect [66]	2,508,470	99.79%
SNN, with STDP [40]	5,017,600	95.0%
Deep SNN with STDP [38]	5,875,456	98.40%
Fully connected SNN, with BP [56]	328,984	98.77%
Convolution SNN with BP [56]	581,520	99.31%
Spiking ConvNet [49]	1,422,848	99.11%
SNN, with NormAD (this work)	81,120	98.17%
ANN, with BP (this work)	81,120	98.0%

360 To benchmark the classification performance of our network, we compare the
361 accuracy and number of learning synapses in other state-of-the-art approaches
362 for MNIST handwritten digit classification (Table 2). We note that while the
363 accuracy of our approach is about 1.6% worse than the best in class approach,
364 our network achieves this accuracy with four to twenty times fewer number of
365 trainable synaptic weights.

366 Table 3 presents the confusion matrix for the SNN based classification of the
367 MNIST test data-sets into 10 classes. It can be seen that for all the digits, the
368 true positive rate is 97% and above, demonstrating the high selectivity of the
369 classifier layer, even though this is not easily discernible from the weight maps
370 (Fig. 8). Only five images failed to elicit any spikes in the output neurons.

Table 3: Confusion matrix for the SNN’s predicted output shows high selectivity of the NormAD trained classifier layer for each digit.

Actual Predicted	0	1	2	3	4	5	6	7	8	9
0	973	0	3	0	2	2	9	1	4	4
1	0	1126	1	0	0	0	2	4	0	4
2	2	3	1015	4	1	1	0	9	1	1
3	0	2	0	996	0	7	1	1	6	4
4	0	1	2	0	964	0	1	1	5	7
5	0	1	0	6	0	876	3	0	1	3
6	2	1	1	0	5	3	940	0	1	0
7	1	1	6	2	0	1	0	1005	3	7
8	1	0	1	1	1	2	1	3	947	3
9	0	0	2	1	9	0	0	3	6	975
No spike	1	0	1	0	0	0	1	1	0	1
Total	980	1135	1032	1010	982	892	958	1028	974	1009

371 5. Network optimization

372 We now discuss the network optimization studies to translate the software
 373 design for energy and memory constrained hardware platforms.

374 5.1. Low precision weight encoding

375 The ability of a network to maintain its accuracy even when the precision
 376 for storing the network parameters is limited, is crucial for efficient hardware
 377 implementations. It has been observed that accuracy degrades significantly
 378 when low-precision weights are used for network emulation. For instance, a 5%
 379 drop in accuracy (with the MNIST data-set) was observed even with 5-bits of
 380 fixed-point precision for the synaptic weights in [67].

381 We test the ability of our SNN and ANN for inference as a function of the
 382 precision of trained weights. We train the weights of both these networks in
 383 double-precision and then measure the inference accuracy by quantizing these
 384 weights, similar to the approach taken in [68] for designing a scalable hardware
 385 solution. The histograms of the weights of our SNN and ANN after training with
 386 NormAD and gradient descent, respectively, are observed to be log-normally dis-
 387 tributed. Our quantization studies showed that dividing the range of weights

388 into linear bins, rather than log-linear bins gives lesser degradation in perfor-
 389 mance. Fig. 9 shows the drop in accuracy for our networks as the number of
 390 levels for representing the trained weights are reduced. It can be seen that
 391 even at 3-bit quantization, the degradation in SNN accuracy is within 1.0% for
 392 $T = 100$ ms compared to the floating point baseline. Further, across all quan-
 393 tization values, the degradation in accuracy of the ANN is slightly worse than
 394 that of the spiking network. It is also worth pointing out that compared to
 395 previous reports such as [67], where the input spike rate was as high as 1500 Hz,
 396 the firing rate in our SNN is in the range of 10 to 300 Hz, which is closer to the
 397 observed biological spike rates. These results hence demonstrate the robustness
 398 of the SNN architecture and its suitability for memory constrained hardware
 399 platforms.

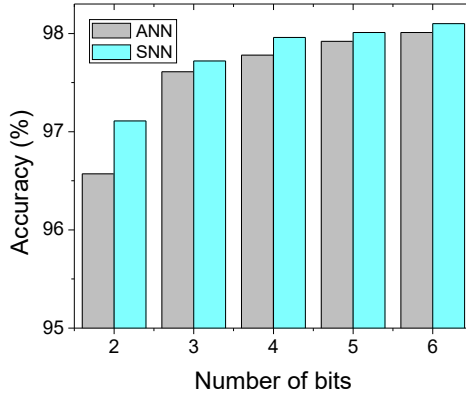


Figure 9: Test accuracy as a function of the precision of the trained weights in the SNN and ANN. Even at 2-bit precision, the SNN accuracy is only about 1% worse than the floating point baseline. Further, the SNN accuracy is better than the corresponding ANN especially at low bit-precision.

400 *5.2. Approximating neuronal dynamics*

401 We also study the SNN’s performance when the dynamics of the neurons is
 402 evaluated with lower precision. As mentioned in the section 3.5, the time step

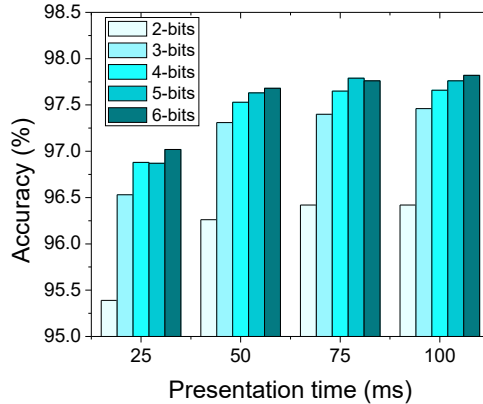


Figure 10: MNIST test accuracy (count metric) as a function of bit-precision of weights and the presentation time T , when the neuronal dynamics is approximated with a larger integration time step of 1 ms. Even at 3-bits of precision and with $T = 50$ ms, the drop in accuracy is within 1% of the baseline.

403 for numerical integration was chosen to be 0.1 ms for learning. Even though
 404 there will be some error in the precise time of spike issue, a larger time step can
 405 be used when the network is used for inference.

406 With $\Delta t = 1$ ms, the neuronal response can be calculated 10 \times faster; Fig. 10
 407 shows the test accuracy as a function of bit-precision and presentation times for
 408 the 3-layer SNN. Here, we used the count metric to determine the test accu-
 409 racy to simplify the computation further. At a bit-precision of 3-bits, the digit
 410 identification can be completed in just 50 ms or with 50 points of neuronal inte-
 411 gration with an accuracy of 97.31%. Hence, close to base-line accuracies can be
 412 maintained in approximate network evaluation that permits higher throughput
 413 for classification.

414 **6. Conclusion and Future Work**

415 We presented a highly compact and efficient 3-layer spiking neural network
 416 for identifying handwritten digits, that achieved an accuracy of 98.17% on the
 417 MNIST data set using the NormAD learning algorithm. All information in the

418 network is encoded and processed in the spike domain at sparse biological spike
419 rates. Our studies show that using the precise time of spike issue for classifica-
420 tion gives slightly better accuracy compared to the simpler rate coding method.
421 We have also presented two techniques to co-optimize the network for hardware
422 implementation, by reducing the bit-precision of weights and approximating the
423 neuronal dynamics with higher integration time-step size.

424 The best convolution networks in both spiking and non-spiking versions that
425 have achieved over 99% accuracy on the MNIST database use at least over
426 300,000 adjustable synapses. The NormAD-trained SNN, on the other hand,
427 has $4\times$ fewer learning parameters, making it amenable for implementation on
428 custom neuromorphic hardware with on-chip learning. Our studies also show
429 that as low as 3-bits of weight precision is sufficient to maintain close to baseline
430 accuracies in the SNN when used for inference. Compared to an equivalent ANN
431 with similar network architecture, the spike based training approach also shows
432 better accuracy, especially at lower precision for synaptic weight storage.

433 The NormAD weight update rule as used in this study can be applied only
434 for tuning the strength of synapses connected to the output layer of a network.
435 However, the methodology used to derive this rule can be extended to adjust the
436 weights of networks with hidden layers in a spike-triggered manner, based on the
437 chain rule of derivatives. Such weight update rules could be then used to pre-
438 train autoencoders which could be stacked and trained to develop deep spiking
439 networks, following the approaches used in deep learning today [5]. Quantifying
440 the performance of such deep spiking networks and determining their accuracy-
441 efficiency trade-offs for large benchmark classification problems is identified as
442 a topic for future exploration.

443 **Acknowledgment**

444 The authors acknowledge valuable discussions with Prof. Osvaldo Simeone
445 at NJIT and Navin Anwani and Bharath Sastha from IIT Bombay. We also
446 gratefully acknowledge the comments of the anonymous reviewers which helped

447 improve the paper.

448 This research was supported in part by the CAMPUSENSE project grant
449 from CISCO Systems Inc; the Semiconductor Research Corporation; and the
450 National Science Foundation grant 1710009. Resources of the High-Performance
451 Computing facility at NJIT was used in this work.

452 **References**

453 [1] National academy of engineering - Reverse-engineer the brain, available at
454 <http://bit.ly/1PmsLiX> (2009).

455 [2] D. H. Hubel, T. N. Wiesel, Receptive fields and functional architecture of
456 monkey striate cortex, *The Journal of physiology* 195 (1) (1968) 215–243.

457 [3] Y. Lecun, L. Bottou, Y. Bengio, P. Haffner, Gradient-based learning ap-
458 plied to document recognition, *Proceedings of the IEEE* 86 (11) (1998)
459 2278–2324. [doi:10.1109/5.726791](https://doi.org/10.1109/5.726791).

460 [4] D. Ciregan, U. Meier, J. Schmidhuber, Multi-column deep neural networks
461 for image classification, in: *2012 IEEE Conference on Computer Vision*
462 and *Pattern Recognition*, 2012, pp. 3642–3649. [doi:10.1109/CVPR.2012.6248110](https://doi.org/10.1109/CVPR.2012.6248110).

463 [5] G. E. Hinton, S. Osindero, Y.-W. Teh, A fast learning algorithm for deep
464 belief nets, *Neural computation* 18 (7) (2006) 1527–1554.

465 [6] A. Krizhevsky, I. Sutskever, G. E. Hinton, ImageNet Classification with
466 deep convolutional neural networks, in: F. Pereira, C. J. C. Burges, L. Bot-
467 tou, K. Q. Weinberger (Eds.), *Advances in Neural Information Processing*
468 *Systems* 25, Curran Associates, Inc., 2012, pp. 1097–1105.

469 [7] Y. Goldberg, A primer on neural network models for natural language
470 processing., *J. Artif. Intell. Res.(JAIR)* 57 (2016) 345–420.

472 [8] G. Hinton, L. Deng, D. Yu, G. E. Dahl, A. R. Mohamed, N. Jaitly, A. Se-
473 nior, V. Vanhoucke, P. Nguyen, T. N. Sainath, B. Kingsbury, Deep Neural
474 Networks for Acoustic Modeling in Speech Recognition: The Shared Views
475 of Four Research Groups, *IEEE Signal Processing Magazine* 29 (6) (2012)
476 82–97. [doi:10.1109/MSP.2012.2205597](https://doi.org/10.1109/MSP.2012.2205597).

477 [9] A. Karpathy, G. Toderici, S. Shetty, T. Leung, R. Sukthankar, L. Fei-Fei,
478 Large-scale Video Classification with Convolutional Neural Networks, in:
479 2014 IEEE Conference on Computer Vision and Pattern Recognition, 2014,
480 pp. 1725–1732. [doi:10.1109/CVPR.2014.223](https://doi.org/10.1109/CVPR.2014.223).

481 [10] I. Goodfellow, Y. Bengio, A. Courville, Deep Learning.
482 URL <http://www.deeplearningbook.org>

483 [11] I. Goodfellow, D. Warde-Farley, M. Mirza, A. Courville, Y. Bengio, Max-
484 out networks, in: S. Dasgupta, D. McAllester (Eds.), *Proceedings of the*
485 *30th International Conference on Machine Learning*, Vol. 28 of *Proceedings*
486 *of Machine Learning Research*, PMLR, Atlanta, Georgia, USA, 2013, pp.
487 1319–1327.
488 URL <http://proceedings.mlr.press/v28/goodfellow13.html>

489 [12] W. Maass, Networks of spiking neurons: The third generation of
490 neural network models, *Neural networks* 10 (9) (1997) 1659–1671, =
491 <http://www.sciencedirect.com/science/article/pii/S0893608097000117>.
492 [doi:10.1016/S0893-6080\(97\)00011-7](http://dx.doi.org/10.1016/S0893-6080(97)00011-7).

493 [13] R. Gutig, H. Sompolinsky, The tempotron: a neuron that learns spike
494 timing-based decisions, *Nat Neurosci* 9 (3) (2006) 420–428. [doi:10.1038/nn1643](https://doi.org/10.1038/nn1643).

496 [14] J. M. Brader, W. Senn, S. Fusi, Learning Real-World Stimuli in a Neu-
497 ral Network with Spike-Driven Synaptic Dynamics, *Neural Computation*
498 19 (11) (2007) 2881–2912. [doi:10.1162/neco.2007.19.11.2881](https://doi.org/10.1162/neco.2007.19.11.2881).

499 [15] J. J. Hopfield, C. D. Brody, Learning rules and network repair in spike-
500 timing-based computation networks, *Proceedings of the National Academy of Sciences* 101 (1) (2004) 337–342. doi:10.1073/pnas.2536316100.

502 [16] P. Crotty, W. B. Levy, Energy-efficient interspike interval codes, *Neurocomputing* 65 (2005) 371 – 378, Computational Neuroscience: Trends in Research 2005. doi:<http://dx.doi.org/10.1016/j.neucom.2004.10.031>.

505 [17] F. Gabbiani, W. Metzner, Encoding and processing of sensory information
506 in neuronal spike trains, *Journal of Experimental Biology* 202 (10) (1999)
507 1267–1279. arXiv:<http://jeb.biologists.org/content/202/10/1267.full.pdf>.

509 [18] S. Shoham, D. H. O'Connor, R. Segev, How silent is the brain: is there a
510 “dark matter” problem in neuroscience?, *Journal of Comparative Physiology A* 192 (8) (2006) 777–784. doi:10.1007/s00359-006-0117-6.

512 [19] A. Roxin, N. Brunel, D. Hansel, G. Mongillo, C. van Vreeswijk,
513 On the distribution of firing rates in networks of cortical neurons,
514 *Journal of Neuroscience* 31 (45) (2011) 16217–16226. arXiv:<http://www.jneurosci.org/content/31/45/16217.full.pdf>, doi:10.1523/JNEUROSCI.1677-11.2011.
516
517 URL <http://www.jneurosci.org/content/31/45/16217>

518 [20] B. Wang, W. Ke, J. Guang, G. Chen, L. Yin, S. Deng, Q. He, Y. Liu,
519 T. He, R. Zheng, Y. Jiang, X. Zhang, T. Li, G. Luan, H. D. Lu, M. Zhang,
520 X. Zhang, Y. Shu, Firing frequency maxima of fast-spiking neurons in hu-
521 man, monkey, and mouse neocortex, *Frontiers in Cellular Neuroscience* 10
522 (2016) 239, 27803650[pmid]. doi:10.3389/fncel.2016.00239.

523 [21] P. A. Merolla, J. V. Arthur, R. Alvarez-Icaza, A. S. Cassidy, J. Sawada,
524 F. Akopyan, B. L. Jackson, N. Imam, C. Guo, Y. Nakamura, B. Brezzo,
525 I. Vo, S. K. Esser, R. Appuswamy, B. Taba, A. Amir, M. D. Flickner, W. P.
526 Risk, R. Manohar, D. S. Modha, A million spiking-neuron integrated circuit

527 with a scalable communication network and interface, *Science* 345 (6197)
528 (2014) 668–673. doi:10.1126/science.1254642.

529 [22] J. Gehlhaar, Neuromorphic Processing: A New Frontier in Scaling Com-
530 puter Architecture, in: Proceedings of the 19th International Confer-
531 ence on Architectural Support for Programming Languages and Operating
532 Systems, ASPLOS '14, ACM, New York, NY, USA, 2014, pp. 317–318.
533 doi:10.1145/2541940.2564710.

534 [23] N. Qiao, H. Mostafa, F. Corradi, M. Osswald, F. Stefanini, D. Sumislawski,
535 G. Indiveri, A reconfigurable on-line learning spiking neuromorphic proces-
536 sor comprising 256 neurons and 128k synapses, *Frontiers in Neuroscience* 9
537 (2015) 141. doi:10.3389/fnins.2015.00141.

538 [24] S. B. Furber, F. Galluppi, S. Temple, L. A. Plana, The SpiNNaker project,
539 Proceedings of the IEEE 102 (5) (2014) 652–665. doi:10.1109/JPROC.
540 2014.2304638.

541 [25] B. V. Benjamin, P. Gao, E. McQuinn, S. Choudhary, A. R. Chan-
542 drasekaran, J. M. Bussat, R. Alvarez-Icaza, J. V. Arthur, P. A. Merolla,
543 K. Boahen, Neurogrid: A Mixed-Analog-Digital Multichip System for
544 Large-scale Neural Simulations, Proceedings of the IEEE 102 (5) (2014)
545 699–716. doi:10.1109/JPROC.2014.2313565.

546 [26] F. Ponulak, A. Kasinski, Supervised Learning in Spiking Neural Net-
547 works with ReSuMe: Sequence Learning, Classification, and Spike Shift-
548 ing, *Neural Computation* 22 (2) (2010) 467–510. doi:10.1162/neco.2009.
549 11-08-901.

550 [27] S. M. Bohte, J. N. Kok, H. La Poutre, Error-backpropagation in temporally
551 encoded networks of spiking neurons, *Neurocomputing* 48 (1) (2002) 17–37.
552 doi:[http://dx.doi.org/10.1016/S0925-2312\(01\)00658-0](http://dx.doi.org/10.1016/S0925-2312(01)00658-0).

553 [28] A. Mohammed, S. Schliebs, S. Matsuda, N. Kasabov, SPAN: Spike Pat-
554 tern Association Neuron for Learning Spatio-Temporal Spike Patterns, In-

555 International Journal of Neural Systems 22 (04), pMID: 22830962. doi:
556 10.1142/S0129065712500128.

557 [29] Q. Yu, H. Tang, K. C. Tan, H. Li, Precise-Spike-Driven Synaptic Plasticity:
558 Learning Hetero-Association of Spatiotemporal Spike Patterns, PLOS ONE
559 8 (11) (2013) 1–16. doi:10.1371/journal.pone.0078318.

560 [30] R. V. Florian, The chronotron: A Neuron That Learns to Fire Temporally
561 Precise Spike Patterns, PloS ONE 7 (8) (2012) e40233. doi:<https://doi.org/10.1371/journal.pone.0040233>.

563 [31] M. Mozafari, S. R. Kheradpisheh, T. Masquelier, A. Nowzari-Dalini,
564 M. Ganjtabesh, First-spike based visual categorization using reward-
565 modulated stdp, arxiv preprint arXiv:1705.09132 [q-bio.NC].

566 [32] A. Taherkhani, A. Belatreche, Y. Li, L. P. Maguire, DL-ReSuMe: A Delay
567 Learning-Based Remote Supervised Method for Spiking Neurons, IEEE
568 Transactions on Neural Networks and Learning Systems 26 (12) (2015)
569 3137–3149. doi:10.1109/TNNLS.2015.2404938.

570 [33] X. Xie, H. Qu, Z. Yi, J. Kurths, Efficient Training of Supervised Spik-
571 ing Neural Network via Accurate Synaptic-Efficiency Adjustment Method,
572 IEEE Transactions on Neural Networks and Learning Systems 28 (6) (2017)
573 1411–1424. doi:10.1109/TNNLS.2016.2541339.

574 [34] J. Tapson, G. Cohen, S. Afshar, K. Stiefel, Y. Buskila, R. Wang, T. J.
575 Hamilton, A. van Schaik, Synthesis of neural networks for spatio-temporal
576 spike pattern recognition and processing, arXiv preprint arXiv:1304.7118.

577 [35] W. W. Lee, S. L. Kukreja, N. V. Thakor, CONE: Convex-Optimized-
578 Synaptic Efficacies for Temporally Precise Spike Mapping, IEEE Trans-
579 actions on Neural Networks and Learning Systems 28 (4) (2017) 849–861.
580 doi:10.1109/TNNLS.2015.2509479.

581 [36] T. Masquelier, S. J. Thorpe, Unsupervised Learning of Visual Features
582 through Spike Timing Dependent Plasticity, PLOS computational biology
583 3 (2) (2007) 1–11. doi:10.1371/journal.pcbi.0030031.

584 [37] P. Panda, K. Roy, Unsupervised regenerative learning of hierarchical fea-
585 tures in spiking deep networks for object recognition, in: 2016 Interna-
586 tional Joint Conference on Neural Networks, 2016, pp. 299–306. doi:
587 10.1109/IJCNN.2016.7727212.

588 [38] S. R. Kheradpisheh, M. Ganjtabesh, S. J. Thorpe, T. Masquelier, STDP-
589 based spiking deep convolutional neural networks for object recogni-
590 tion, Neural Networks doi:<https://doi.org/10.1016/j.neunet.2017.12.005>.

592 [39] A. Tavanaei, A. S. Maida, Multi-layer unsupervised learning in a spiking
593 convolutional neural network, in: 2017 International Joint Conference on
594 Neural Networks (IJCNN), 2017, pp. 2023–2030. doi:10.1109/IJCNN.
595 2017.7966099.

596 [40] P. U. Diehl, M. Cook, Unsupervised learning of digit recognition using
597 spike-timing-dependent plasticity, Frontiers in computational neuroscience
598 9 (2015) 99. doi:10.3389/fncom.2015.00099.

599 [41] S. Roy, A. Basu, An Online Unsupervised Structural Plasticity Algo-
600 rithm for Spiking Neural Networks, IEEE Transactions on Neural Networks
601 and Learning Systems 28 (4) (2017) 900–910. doi:10.1109/TNNLS.2016.
602 2582517.

603 [42] J. M. Allred, K. Roy, Unsupervised incremental STDP learning using forced
604 firing of dormant or idle neurons, in: 2016 International Joint Conference
605 on Neural Networks (IJCNN), 2016. doi:10.1109/IJCNN.2016.7727509.

606 [43] N. K. Kasabov, NeuCube: A spiking neural network architecture for map-
607 ping, learning and understanding of spatio-temporal brain data, Neural

608 Networks 52 (2014) 62–76. doi:<http://dx.doi.org/10.1016/j.neunet.2014.01.006>.

610 [44] N. Kasabov, N. M. Scott, E. Tu, S. Marks, N. Sengupta, E. Capecci,
611 M. Othman, M. G. Daborjeh, N. Murli, R. Hartono, J. I. Espinosa-
612 Ramos, L. Zhou, F. B. Alvi, et al., Evolving spatio-temporal data ma-
613 chines based on the NeuCube neuromorphic framework: design methodol-
614 ogy and selected applications, Neural Networks 78 (2016) 1–14. doi:<http://dx.doi.org/10.1016/j.neunet.2015.09.011>.

616 [45] J. Wang, A. Belatreche, L. P. Maguire, T. M. McGinnity, SpikeTemp: An
617 Enhanced Rank-Order-Based Learning Approach for Spiking Neural Net-
618 works with Adaptive Structure, IEEE Transactions on Neural Networks and
619 Learning Systems 28 (2017) 30–43. doi:[10.1109/TNNLS.2015.2501322](https://doi.org/10.1109/TNNLS.2015.2501322).

620 [46] J. Wang, A. Belatreche, L. P. Maguire, T. M. McGinnity, SpikeComp: An
621 Evolving Spiking Neural Network with Adaptive Compact Structure for
622 Pattern Classification, Springer International Publishing, Cham, 2015, pp.
623 259–267. doi:[10.1007/978-3-319-26535-3_30](https://doi.org/10.1007/978-3-319-26535-3_30).

624 [47] T. Takuya, T. Haruhiko, K. Hiroharu, T. Shinji, A training algorithm for
625 spike sequence in spiking neural networks – a discussion on growing network
626 for stable training performance, in: 2016 12th International Conference on
627 Natural Computation, Fuzzy Systems and Knowledge Discovery, 2016, pp.
628 1773–1777. doi:[10.1109/FSKD.2016.7603446](https://doi.org/10.1109/FSKD.2016.7603446).

629 [48] Y. Cao, Y. Chen, D. Khosla, Spiking deep convolutional neural networks
630 for energy-efficient object recognition, International Journal of Computer
631 Vision 113 (1) (2015) 54–66. doi:[10.1007/s11263-014-0788-3](https://doi.org/10.1007/s11263-014-0788-3).

632 [49] P. U. Diehl, D. Neil, J. Binas, M. Cook, S. C. Liu, M. Pfeiffer, Fast-
633 classifying, high-accuracy spiking deep networks through weight and
634 threshold balancing, in: 2015 International Joint Conference on Neural
635 Networks (IJCNN), 2015, pp. 1–8. doi:[10.1109/IJCNN.2015.7280696](https://doi.org/10.1109/IJCNN.2015.7280696).

636 [50] B. Rueckauer, I.-A. Lungu, Y. Hu, M. Pfeiffer, Theory and tools for the con-
637 version of analog to spiking convolutional neural networks, arXiv preprint
638 arXiv:1612.04052.

639 [51] E. Hunsberger, C. Eliasmith, Training spiking deep networks for neuromor-
640 phic hardware, arXiv preprint arXiv:1611.05141.

641 [52] Hunsberger, Eric, Spiking deep neural networks: Engineered and biological
642 approaches to object recognition, Ph.D. thesis (2018).
643 URL <http://hdl.handle.net/10012/12819>

644 [53] B. Rueckauer, I.-A. Lungu, Y. Hu, M. Pfeiffer, S.-C. Liu, Conversion
645 of continuous-valued deep networks to efficient event-driven networks
646 for image classification, *Frontiers in Neuroscience* 11 (2017) 682.
647 doi:10.3389/fnins.2017.00682.
648 URL <https://www.frontiersin.org/article/10.3389/fnins.2017.00682>

650 [54] T. P. Lillicrap, D. Cownden, D. B. Tweed, C. J. Akerman, Random synaptic
651 feedback weights support error backpropagation for deep learning, *Nature*
652 *Communications* doi:<http://dx.doi.org/10.1038/ncomms13276>.

653 [55] N. Anwani, B. Rajendran, NormAD - Normalized Approximate Descent
654 based supervised learning rule for spiking neurons, in: *International Joint*
655 *Conference on Neural Networks*, 2015, pp. 1–8. doi:10.1109/IJCNN.2015.
656 7280618.

657 [56] J. H. Lee, T. Delbrück, M. Pfeiffer, Training Deep Spiking Neural Networks
658 Using Backpropagation, *Frontiers in Neuroscience* 10 (2016) 508. doi:
659 10.3389/fnins.2016.00508.

660 [57] L. F. Abbott, Lapicque’s introduction of the integrate-and-fire model
661 neuron (1907), *Brain Research Bulletin* 50 (1999) 303–304. doi:[http://dx.doi.org/10.1016/S0361-9230\(99\)00161-6](http://dx.doi.org/10.1016/S0361-9230(99)00161-6).

663 [58] S. Panzeri, N. Brunel, N. K. Logothetis, C. Kayser, Sensory neural codes
664 using multiplexed temporal scales, *Trends in Neurosciences* 33 (3) (2010)
665 111 – 120. [doi:
http://dx.doi.org/10.1016/j.tins.2009.12.001](http://dx.doi.org/10.1016/j.tins.2009.12.001).

666 [59] A. A. Lazar, E. K. Simonyi, L. T. Tóth, Time encoding of bandlimited
667 signals, an overview, in: *Proceedings of Conference on Telecommunication*
668 *Systems, Modeling and Analysis*, Citeseer, 2005.

669 [60] J. Wang, A. Belatreche, L. Maguire, M. McGinnity, Online versus offline
670 learning for spiking neural networks: A review and new strategies, in: *2010*
671 *IEEE 9th International Conference on Cyberntic Intelligent Systems*, 2010,
672 pp. 1–6. [doi:
10.1109/UKRICIS.2010.5898113](https://doi.org/10.1109/UKRICIS.2010.5898113).

673 [61] S. Q. Khan, A. Ghani, M. Khurram, Population coding for neuromorphic
674 hardware, *Neurocomputing* 239 (2017) 153 – 164.

675 [62] A. Calderón, S. Roa, J. Victorino, Handwritten digit recognition using
676 convolutional neural networks and gabor filters, *Proc. Int. Congr. Comput.*
677 *Intell.*, 2003.

678 [63] S. Schreiber, J.-M. Fellous, D. Whitmer, P. Tiesinga, T. J. Sejnowski, A
679 new correlation-based measure of spike timing reliability, *Neurocomputing*
680 52 (2003) 925–931, *computational Neuroscience: Trends in Research* 2003.
681 [doi:
http://dx.doi.org/10.1016/S0925-2312\(02\)00838-X](http://dx.doi.org/10.1016/S0925-2312(02)00838-X).

682 [64] T. Gokmen, Y. Vlasov, Acceleration of Deep Neural Network Training
683 with Resistive Cross-Point Devices: Design Considerations, *Frontiers in*
684 *Neuroscience* 10 (2016) 333. [doi:
10.3389/fnins.2016.00333](https://doi.org/10.3389/fnins.2016.00333).

685 [65] J. Tapson, P. De Chazal, A. van Schaik, Explicit computation of input
686 weights in extreme learning machines, Springer International Publishing,
687 Cham, 2015, pp. 41–49. [doi:
10.1007/978-3-319-14063-6_4](https://doi.org/10.1007/978-3-319-14063-6_4).

688 [66] L. Wan, M. Zeiler, S. Zhang, Y. L. Cun, R. Fergus, Regularization of Neu-
689 *ral Networks using DropConnect*, in: *Proceedings of the 30th International*

690 Conference on Machine Learning, Vol. 28 of Proceedings of Machine Learn-
691 ing Research, PMLR, Atlanta, Georgia, USA, 2013, pp. 1058–1066.
692 URL <http://proceedings.mlr.press/v28/wan13.html>

693 [67] E. Stromatias, D. Neil, M. Pfeiffer, F. Galluppi, S. B. Furber, S.-C. Liu,
694 Robustness of spiking Deep Belief Networks to noise and reduced bit pre-
695 cision of neuro-inspired hardware platforms, *Frontiers in Neuroscience* 9
696 (2015) 222. doi:10.3389/fnins.2015.00222.

697 [68] S. R. Kulkarni, B. Rajendran, Scalable digital CMOS Architecture for Spike
698 based Supervised Learning, Springer International Publishing, Cham, 2015,
699 pp. 149–158. doi:10.1007/978-3-319-23983-5_15.